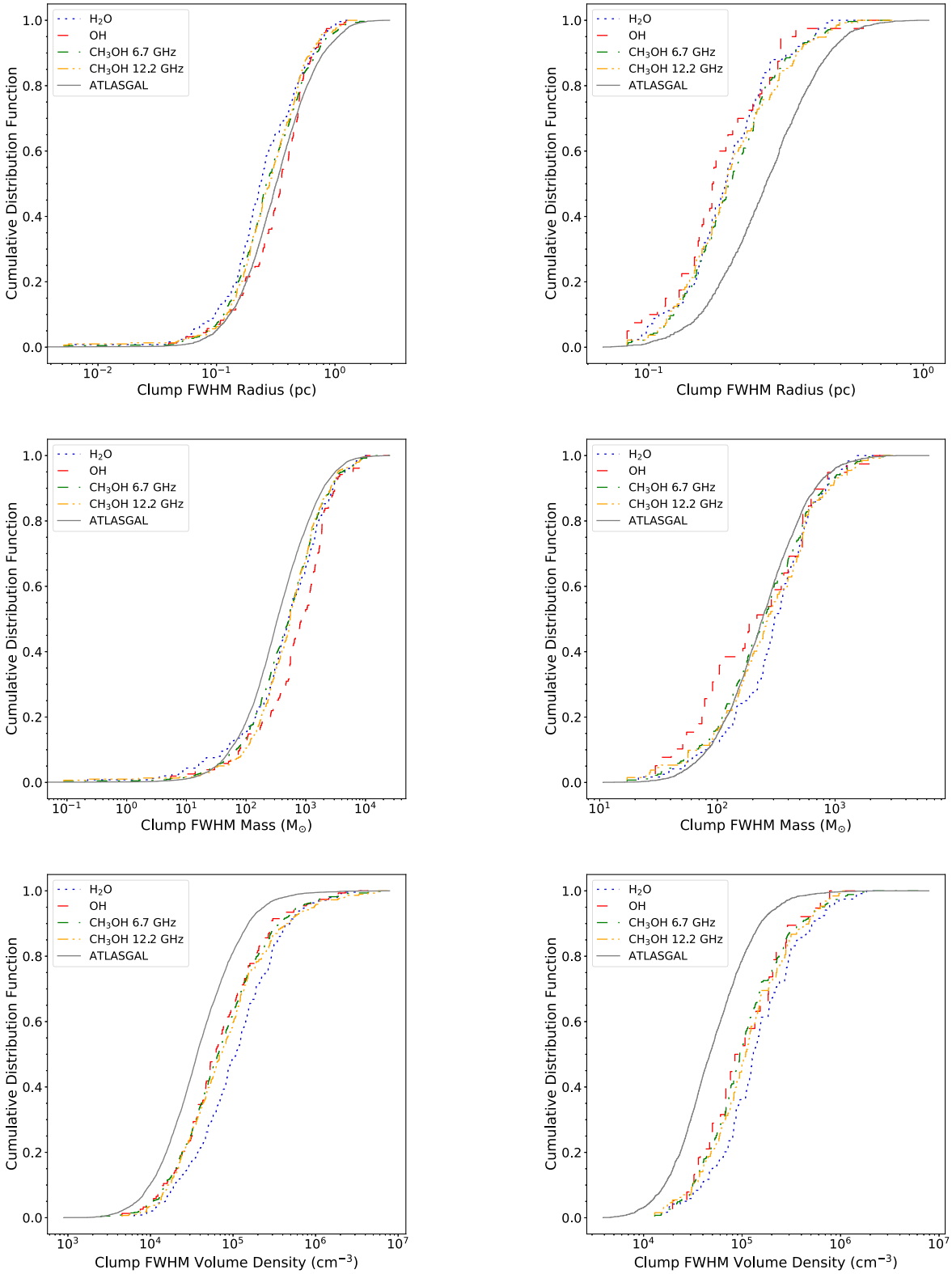

Figure 7. Clump FWHM radius, clump FWHM mass, and clump FWHM volume density distributions are presented in the upper, middle, and lower panels respectively. The cumulative distribution functions in the left-hand panels present the entire distributions of the maser associated clumps and the full ATLASGAL sample, whereas the cumulative distribution functions in the right-hand panels present a distance-limited sample (2–5 kpc) of the same distributions. Legends for each sample presented are shown in the top left-hand corner of each panel.

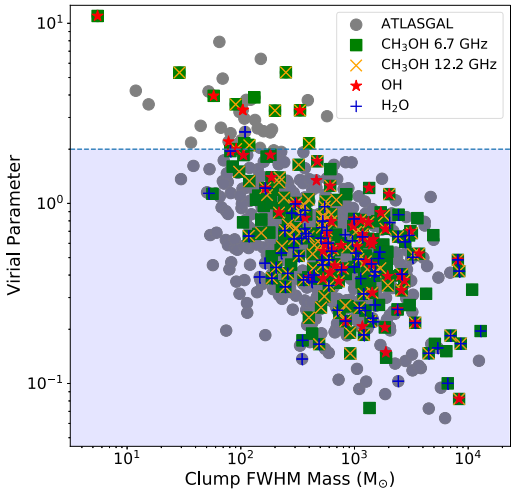

Figure 8. Virial parameters versus clump mass for maser associated clumps. This plot presents a distance-limited sample (2–5 kpc). The blue shaded area indicates the region of parameter space where clumps are gravitationally unstable (virial parameter < 2; Kauffmann, Pillai & Goldsmith 2013).

The virial parameter has been calculated for 741 ATLASGAL clumps (Urquhart et al. 2018). Fig. 8 presents the distribution of these virial parameters against clump FWHM mass for all clumps. We find that the majority of our clumps have a value lower than 2 and so are likely to be unstable to gravitational collapse, and no differing trends are seen between the maser samples.

Free-fall time-scales can be derived for each clump that have a corresponding FWHM volume density measurement

$$t_{\rm ff} = \sqrt{\frac{3\pi}{32G\rho}}, \tag{3}$$

where ρ is the mean volume density of a clump and G is the gravitational constant. The free-fall times for sources detected in ATLASGAL range between $\sim 2 \times 10^4$ and 2×10^6 yr. These free-fall times will be used to derive the statistical lifetime for each maser species in Section 5.2.2. When calculating the free-fall times of clumps, we have assumed that the dominant force is gravity and have not taken into account any support mechanisms that may impede the global collapse of clumps. However, given that ∼90 per cent of ATLASGAL clumps are associated with star formation it is safe to assume they are collapsing locally if not globally (Urquhart et al. 2018).

4.3 Maser and Bolometric luminosities

Maser luminosities have been calculated using the determined flux density values from the respective maser surveys and distance measurements taken from Urquhart et al. (2018). For consistency, we have used the peak maser fluxes rather than the integrated fluxes to determine the maser luminosities, as the Walsh et al. (2014) HOPS catalogue does not contain integrated fluxes as they focused on the distribution of individual maser spots. In Billington et al. (2019), we show that the differences between the peak and integrated fluxes for maser emission are insignificant above 1 Jy. The maser luminosities have units of Jy kpc^2 km s^{-1} and are, therefore, somewhat arbitrary. As in Billington et al. (2019), we have used conversion factors to convert the maser luminosities into solar units, a list of these factors can be found in Table 4 (see section 4.5 of Billington et al. 2019). The distribution of maser luminosities can be seen in Fig. 9. We find that the methanol and water masers have similar luminosities whereas

Table 4. Factors for converting the maser luminosities into units of L$_\odot$.

Maser transition frequency	Conversion factor (kHz)
22.235-GHz	74.1
1612-MHz	5.4
1665-MHz	5.6
1667-MHz	5.6
1720-MHz	5.7
6.7-GHz	22.3
12.2-GHz	40.7

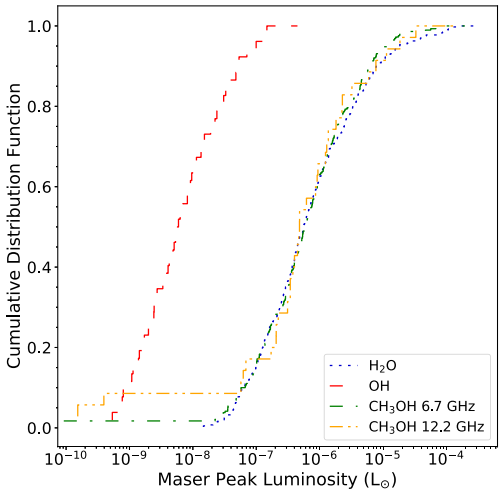

Figure 9. Cumulative distribution function showing a distance-limited samples (2–5 kpc) of the maser luminosities for all the species. The legend of each species is given the lower right-hand side of the plot.

the hydroxyl masers are significantly less luminous. Previous studies have also found similar results (e.g. Szymczak et al. 2005). This is expected as it has been theorized that OH masers are associated with the expanding material around H II regions. This material is less dense and so OH maser emission is weaker (Forster & Caswell 1989).

Bolometric luminosities have been taken unchanged from Urquhart et al. (2018). These luminosities have been calculated by reconstructing each sources' SED. A more detailed analysis of this method can be found in section 3 of König et al. (2017). Fig. 10 presents the distribution of luminosities as cumulative distribution functions (full sample and distance-limited sample). There appears to be no significant trends or differences between clumps associated with the different types of masers. Although they do appear to be significantly more luminous when compared to the full sample of clumps; this will be discussed in detail in Section 5.2.

4.4 Temperatures and $L_{\rm bol}/M_{\rm fwhm}$ ratios

Along with the physical parameters that have been derived in the previous subsections, we also define the $L_{\rm bol}/M_{\rm fwhm}$ ratio. This is the ratio between the bolometric luminosity of clumps and their corresponding FWHM mass, a distance independent quantity. Previous works have shown that this ratio is a good indicator of the evolutionary stage (Molinari et al. 2008, 2019), and so for the analysis within this study we shall use the $L_{\rm bol}/M_{\rm fwhm}$ ratios of clumps to determine the global evolutionary phase of these star formation regions. The $L_{\rm bol}/M_{\rm fwhm}$ ratios for the ATLASGAL sample range from $10^{-2.4}$ to $10^{3.3}$ L$_\odot$/M$_\odot$ with a mean of $10^{0.4}$ L$_\odot$/M$_\odot$. Fig. 11 presents the $L_{\rm bol}/M_{\rm fwhm}$ ratio

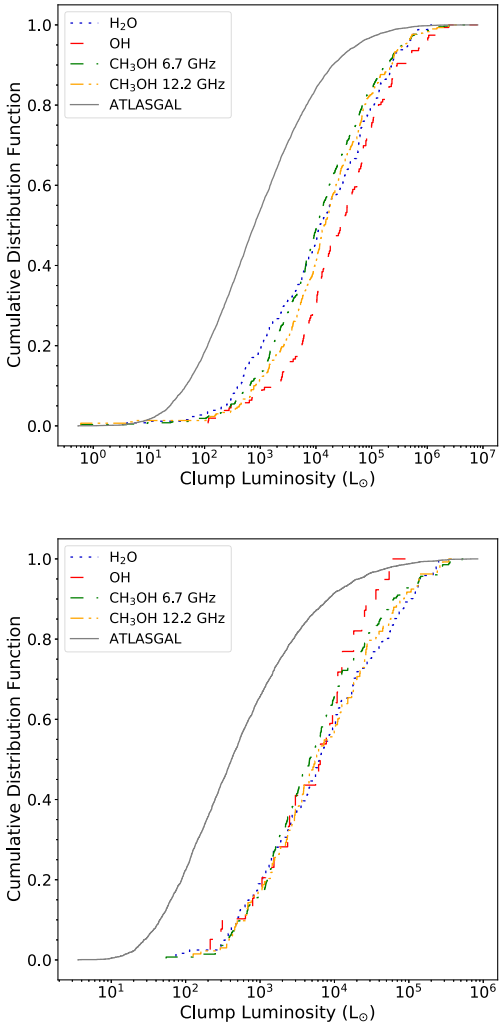

Figure 10. Clump luminosity parameter distributions. The cumulative distribution function in the upper panel presents the entire distribution of the maser associated clumps and the full ATLASGAL sample. The cumulative distribution function in the lower panel presents a distance-limited sample (2–5 kpc). Legends for each maser associated clump are given in the upper top left-hand side of both panels.

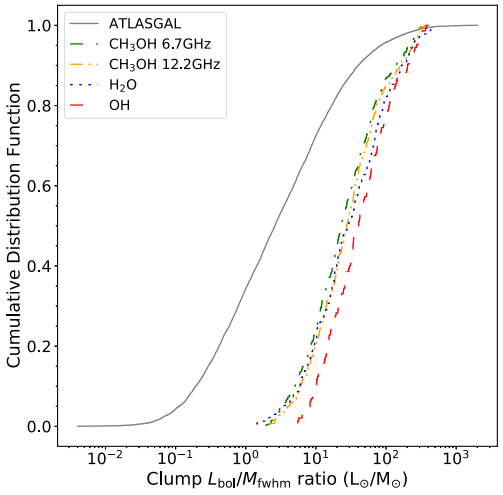

Figure 11. The cumulative distribution function of the $L_{\rm bol}/M_{\rm fwhm}$ ratios for all maser associated clumps. A legend is shown in the top left-hand side for each of the subsamples.

distributions as a cumulative distribution function, which will be further discussed in Section 5.2.1.

Temperatures for all clumps have also been utilized from the ATLASGAL survey (Urquhart et al. 2018). Along with the $L_{\rm bol}/M_{\rm fwhm}$ ratios, temperature is a good indicator of evolution as it has been shown that temperature and $L_{\rm bol}/M_{\rm fwhm}$ ratios of Galactic clumps are tightly correlated (see fig. 22 of Urquhart et al. 2018).

4.5 Uncertainties in physical parameters

The uncertainties in the distance measurements towards clumps are of the order of ±0.5 kpc and are estimated from the Bayesian distance algorithm presented in Reid et al. (2016). The uncertainty for radius is linearly correlated with the distance errors and this uncertainty is ∼30 per cent at 1 kpc but only a few percent at distances larger than 10 kpc. The mean error found when determining the dust temperature values from the SEDs is ∼10 per cent. The fractional uncertainty for the maser luminosities is roughly $\sqrt{2}$ times the fractional uncertainty in the distance measurements. However, in calculating this quantity we are assuming the maser sources are emitting isotropically and so the uncertainty for these measurements are hard to estimate. As for the physical properties of the clumps, the error in the bolometric luminosities is a factor of a few due to the uncertainty on the bolometric flux values (15–50 per cent, depending on the wavelength of the observations; see König et al. 2017) and the distance errors. The uncertainty in the mass and volume density are likely dominated by the uncertainty in the value for the dust absorption coefficient (interpolated from Schuller et al. 2009 and taken to be 1.85 cm^2 g^{-1}) and the estimation of the dust-to-gas ratio (taken to be 100). Both of these parameters are poorly constrained and lead to uncertainties of a factor of ∼2–3. The uncertainties on the $L_{\rm bol}/M_{\rm fwhm}$ ratios are also a factor of a few, following the errors on the luminosity and mass calculations.

While the uncertainties in the physical parameters may be quite large, they affect the entire sample uniformly and will increase the scatter in the distributions. However, this will still allow for statistical trends to be identified and analysed, especially when considering a distance-limited sample. The use of a distance-limited sample will reduce biases of mass and size due to sensitivity limitations and the large range of distances to the clumps.

5 DISCUSSION

As in Billington et al. (2019), we have opted to only use the central 95 per cent (2σ) of parameter values within any given distribution. This will remove any potential errors or biases resulting from outliers due to inaccurate distance measurements or extreme sources.

5.1 Analysis tool: Kolmogorov–Smirnov test

Throughout this work, we employ the use of a two-sample Kolmogorov–Smirnov (KS) test. A two-sample KS test is a non-parametric test that compares the empirical cumulative distribution functions for two samples. The test measures the largest difference between two distributions and the associated confidence value, referred to as a p-value. The null hypothesis is that two samples are drawn from the same parent population. However, the null hypothesis can be rejected if the p-value is smaller than a selected confidence threshold (taken here as 3σ; i.e. $p < 0.0013$). This allows us to conclude that there is sufficient evidence to consider the samples

Table 5. The central 95 per cent of the $L_{\rm bol}/M_{\rm fwhm}$ ratio, volume density (distance limited), and luminosities (distance limited) parameters for each maser species.

Maser species	$L_{\rm bol}/M_{\rm fwhm}$ ratio ranges	Volume density ranges ($\rm cm^{-3}$)	Luminosity ranges ($\rm L_\odot$)
Water	$10^{0.15}-10^{2.66}$	$10^{4.5}-10^{6.3}$	$10^{2.6}-10^{5.4}$
Hydroxyl	$10^{0.74}-10^{2.59}$	$10^{4.4}-10^{5.9}$	$10^{2.5}-10^{5.1}$
Methanol 12.2-GHz	$10^{0.32}-10^{2.60}$	$10^{4.2}-10^{6.0}$	$10^{2.6}-10^{5.4}$
Methanol 6.7-GHz	$10^{0.27}-10^{2.57}$	$10^{4.1}-10^{6.0}$	$10^{2.5}-10^{5.4}$

to be drawn from different populations and that two samples are significantly different from each other.

5.2 Physical parameters

Fig. 7 presents the full sample and distance-limited sample cumulative distribution functions of clump FWHM radius, FWHM mass, and FWHM volume density. It can be seen that the clumps associated with a maser are more compact than the full ATLASGAL sample, as presented in the upper right-hand panel of Fig. 7. The ratio between the mean clump radii for maser clumps versus non-maser clumps is 0.85. A two-sample KS test has also been applied to the radii of clumps associated with a maser source and the ATLASGAL sample to identify whether the difference in radii between the two samples is statistically significant. This has revealed that all of the maser associated clumps are significantly more compact than the rest of the dust clump sample ($p \ll 0.0013$).

We have also assessed the differences in temperature between clumps hosting a maser and those that do not. As can be seen in Table 3, clumps with associated maser emission are warmer than their non-maser counterparts. The mean temperature of a maser clump is 23.9 K whereas the mean temperature of an ATLASGAL clump is 19.4 K. We have also tested the samples using a KS test and find that the differences in temperature between the two samples is statistically significant ($p \ll 0.0013$). This difference has also been noted in another previous study by Jones et al. (2020), who examined a sample of 731 MMB sources with compact emission at four Hi-GAL wavelengths, and investigated the association between masers and Hi-GAL sources.

The masses of maser associated clumps are similar to the average mass of dense clumps and we do not find any significant differences, as confirmed by a KS test. As the clumps containing a maser are significantly more compact than the ATLASGAL sample, while having similar masses, the calculated volume densities are naturally increased. This shows that all maser species of interest are only associated with those clumps above a certain density threshold ($n(\rm H_2) > 10^{4.1}\,cm^{-3}$); this density limit is consistent with the result found in Billington et al. (2019) for the 6.7-GHz methanol masers.

Fig. 10 presents the distribution of clump luminosity for our various samples and we find that all of the maser clumps are more luminous by a factor of approximately 10 when compared to the average clump luminosity. The mean and median luminosities for maser associated clumps are both $\sim 10^4\,\rm L_\odot$. These values are ~ 2 times higher than those found by Jones et al. (2020), likely due to the differences in the way that the luminosity measurements were conducted. This implies that a certain protostellar luminosity is required, and therefore, protostellar mass in order to drive sufficient radiative and mechanical energy into the circumstellar environment to effectively pump the various maser species.

The physical parameters discussed above are all similar for each of the clumps associated with a different maser species, and all appear to be significantly larger when compared to the full ATLASGAL sample, except clump radius. These results do not completely conform with previous studies. For example, Breen & Ellingsen (2011) found that water masers are typically found towards clumps with larger radii, increased mass and increased luminosity. While we do find that masers are associated with clumps of increased luminosity, these clumps are found to be more compact than the larger ATLASGAL sample, and also have similar masses. This conflict is likely to be due to the source sample used in Breen et al. (2010), which originates from Hill et al. (2005). This millimetre study presented observations of 131 star-forming complexes suspected of harbouring massive star formation. The statistically significant differences between the samples presented in this study and Hill et al. (2005) can be attributed to the method of calculating the radii and masses of individual sources. The radii of millimetre sources in Hill et al. (2005) is highly dependent on the temperature of each region, an observational bias that is described in Billington et al. (2019), and instead we chose to calculated the sizes of sources based on the FWHM flux distribution. Moreover, Hill et al. (2005) used a constant temperature of 20 K to determine the mass of each clump, whereas the ATLASGAL temperatures are based on the results of SEDs, we therefore consider our results to be more reliable.

5.2.1 *Evolutionary Stage – L_{bol}/M_{fwhm} ratios*

Fig. 11 presents the cumulative distribution function for the $L_{\rm bol}/M_{\rm fwhm}$ ratios of all the maser species and the full ATLASGAL sample. It can be seen from this Figure, that all the maser species occupy approximately the same distinct part of the parameter space, between $\sim 10^{0.2}$ and $10^{2.7}\,\rm L_\odot/M_\odot$. The exact ranges of the $L_{\rm bol}/M_{\rm fwhm}$ ratios for each maser species can be found in Table 5.

We have tested the $L_{\rm bol}/M_{\rm fwhm}$ ratios using clumps that have masses of $>500\,\rm M_\odot$ and by only using the clumps with the smallest offsets to their associated maser sources (spatial offset <10 arcsec, velocity offset $<5\,\rm km\,s^{-1}$). We find that these restrictions have no effect on the overall distributions of the $L_{\rm bol}/M_{\rm fwhm}$ ratios for each maser sample, and the corresponding $L_{\rm bol}/M_{\rm fwhm}$ ratio ranges. Since the $L_{\rm bol}/M_{\rm fwhm}$ ratios of all of the maser associated clumps are similar (as confirmed by a KS test), this suggests that the mechanisms required for the production of any maser emission only occurs at a set stage in the evolution of star formation and then only for protostellar sources above a certain luminosity ($\sim 500\,\rm L_\odot$).

In Fig. 12 we show clump FWHM volume density versus clump $L_{\rm bol}/M_{\rm fwhm}$ ratio. It can be seen that there is a slight negative correlation between these two parameters. Although, this is likely to be due to the sensitivity limit of the ATLASGAL survey, which is also shown in the Figure. In Billington et al. (2019), a lower limit of volume density for 6.7-GHz methanol maser associated clumps was found to be $10^{4.1}\,\rm cm^{-3}$. This limit seems to hold for all of the maser species presented in this study, as shown in Fig. 12 and Table 5. Overall, our results show that certain physical conditions are necessary for the presence of any type of maser. These conditions are as follows: $L_{\rm bol}/M_{\rm fwhm}$ of between $10^{0.2}$ and $10^{2.7}$, volume densities of above